BLADE DESIGN AND OPTIMIZATION OF LOW PRESSURE AXIAL FANS USING A CASCADE APPROACH

Heiko WINTERBERG [1], Jens FRIEDRICHS [2]

[1] *Volkswagen AG, Engine Cooling Developement, Brieffach 011/1750, 38440 Wolfsburg, Germany*

[2] *TU Braunschweig, Institute of Jet Propulsion and Turbomachinery, 38108 Braunschweig, Germany*

SUMMARY

Intermediate solidity axial fans ($0.4 \leq \sigma \leq 1.2$) can often be found in heating, ventilation and air conditioning (HVAC) systems. In many applications (e.g. automotive cooling fans) the aerodynamic design aims for high flow rates at low pressure rises. Therefore those fans usually have no stator, a low hub-to-tip ratio (≤ 0.4) and few blades. While the literature commonly refers to using the isolated airfoil approach for designing those fans, the present paper uses a fully virtual cascade-based approach with subsequent optimization using methods of Response Surface Modelling (RSM) in order to get high efficiency rotor only axial fans with highly swept blades.

INTRODUCTION

Axial fans move air parallel to the rotating machine axis. Especially due to their compact axial design, high efficiency and low noise-levels they are used in a very wide range of applications and scales, from cooling the smallest electrical parts with micro-size rotors to large ventilation systems in heavy industrial facilities. Although this leads to a wide variety of available and possible designs, the basic design-idea is identical: proper selection and stacking of two-dimensional airfoils along the blade-span. Since HVAC type fans usually aim for high flow rates at low pressure rises, an additional stator is often not necessary. In order to get the air moving through the impeller, a total pressure rise is mandatory. To achieve this, the fan-blades have to generate flow-deflection. Therefore the main aerodynamic problem is to predict the needed flow-deflection and find a 2d profile (e.g. airfoil) which is able to achieve this in an efficient way.

In case of low solidities (chord length to pitch ratios) the isolated airfoil approach is commonly used and considered valid due neglectible aerodynamic cascade effects. This technique uses the assumption of idealized flow around an isolated airfoil without taking cascade effects into account.

Eq. (1) shows the basis for the isolated airfoil approach, which couples aerodynamic quantities with geometric parameters (blade solidity). The full derivation of this equation can be found in literature (e.g. [1, 2])

$$C_L \cdot \frac{c}{t} = \frac{Y}{w_\infty \cdot u \cdot \left(1 + \frac{\varepsilon}{\tan \beta_\infty}\right)} \tag{1}$$

On the other side cascade based methods, which take interference effects into account, are widely used in highly stressed applications with medium-to-high solidities. Therefore Lieblein collected data for NACA65 type airfoils in terms of optimal incidence and deviation angles, as well as several additional corrections. [3]

Since the flow deflection is a function of the total pressure rise, fan-manufacturers often have to deal with low flow deflections and intermediate solidities in HVAC-type fans. Cascade data (e.g. those from Lieblein) does not cover small flow deflection. For those cases the literature mostly refers to corrections of the isolated airfoil data to take interference effects at regions of higher solidities into account. [1, 4]

Table 1: Main characteristics of the fan rotor

	symbol	value
Tip radius	r_{tip}	0.2 m
Hub-to-tip ratio	$r_{\text{hub}}/r_{\text{tip}}$	0.4
Total-to-static pressure rise	Δp_{ts}	230 Pa
Volumetric flow rate	$\dot{V}$	2500 m³/h
Speed	n	2680 rpm
No. of blades	N	7

This paper presents a fully virtual design process using the example of a 400 mm rotor-only type cooling fan. The main characteristics can be found in table 1 and a typical 3d-model is shown in fig. 1.

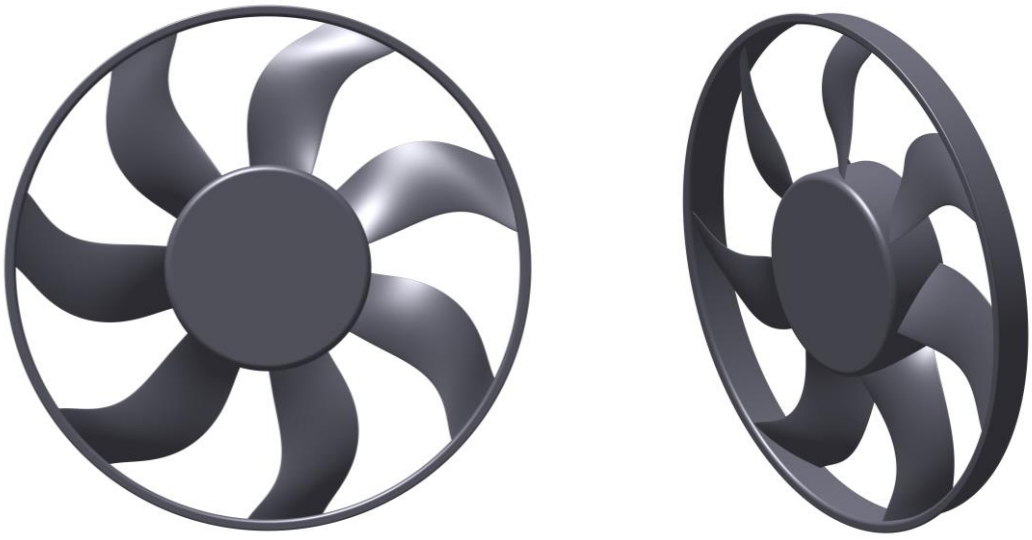

Figure 1: Typical rotor only automotive cooling fan rotor with forward swept blades

DESIGN STRATEGY

Overview

The aerodynamic design strategy is an iterative procedure for rotor-only axial fans. The described vectors, basic parameters and angles are defined in figure 2. Unless otherwise stated all equations are formulated in a 3d-cylindrical (r, θ, z) coordinate system, where r defines the radius from origin, θ the azimuth and z the axis of rotation. The indices "1" and "2" describe the stations in front of (inlet, suction side) and behind (outlet, pressure side) the rotor.

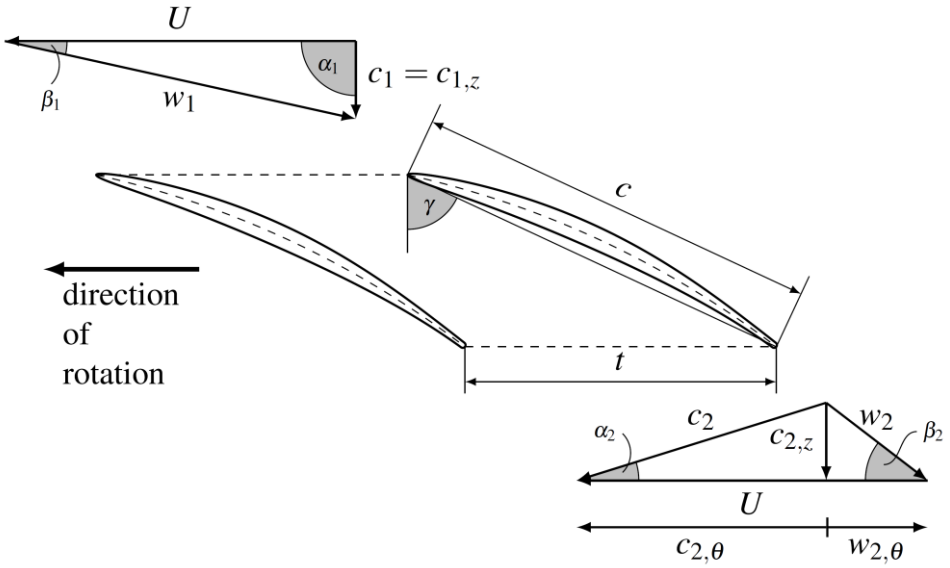

Figure 2: Definition of the basic velocities and angles in front of and behind the rotor shown on a 2d-cascade

The process can be summarized as follows:

1. Input of characteristic design values
2. Computation of the velocity triangles at inlet and outlet using a general controlled vortex approach in combination with radial equilibrium assumptions
3. Determination of the best efficiency airfoil data (e.g. incidence, deviation, loss coefficient) based on cascade simulations
4. Generation and stacking of two-dimensional blade-sections allowing for a flexible incorporation of blade sweep
5. Aerodynamic load corrections to take blade-sweep into account

The aim of this design procedure is to get high efficiency fans with fixed tip and hub diameters within minutes in order to obtain a good initial point for further three-dimensional optimization. To simplify the process as much as possible, some basic assumptions are made:

- incompressible flow due to low Ma-numbers and pressure ratios
- pure axial inflow → $c_{1,\theta} = 0$
- radial velocity components are zero far upstream and downstream of the rotor

Radial Equilibrium

The radial equilibrium describes a balance between radial forces acting upon a moving fluid particle. Therefore the radial pressure force must have the same magnitude as the centrifugal force in the opposite direction as expressed in eq. (2).

$$\frac{1}{\rho}\frac{\partial p}{\partial r} - \frac{c_\theta^2}{r} = 0 \tag{2}$$

Using the definition of total pressure $p_\mathrm{t} = p + 0.5\rho c^2$ and assuming a negligible small radial velocity gradient $\partial c_r/\partial r \approx 0$ we obtain an equation for the axial velocity c_z

$$\frac{\partial c_z^2}{\partial r} = \frac{2}{\rho}\frac{\partial p_\mathrm{t}}{\partial r} - \frac{1}{r^2}\frac{\partial (c_\theta r)^2}{\partial r} \tag{3}$$

According to the Euler equation for turbomachinery the total pressure rise is a function of the flow deflection

$$\left.\frac{\partial p_\mathrm{t}}{\partial r}\right|_2 = \rho\Omega\left(\frac{\partial\left(c_{2,\theta} r\right)}{\partial r} - \frac{\partial\left(c_{1,\theta} r\right)}{\partial r}\right) + \left.\frac{\partial p_\mathrm{t}}{\partial r}\right|_1 \tag{4}$$

Equation (4) can be further simplified if the flow at inlet is 1.) swirl free ($c_{1,\theta} r = 0$) and 2.) total pressure is constant with respect to the radius ($\partial p_t/\partial r = 0$).

By setting the constraint of continuity at a fixed target flowrate

$$\dot{V} = \int c_{1,z}(r)\,\mathrm{d}A = \int c_{2,z}(r)\,\mathrm{d}A \tag{5}$$

and inserting eq. (4) into eq. (3) and integration from hub to tip radius, $c_{2,z}$ becomes a function of the design swirl distribution.

A common design choice is to use some kind of power law swirl distribution [5], for example

$$r c_{2,\theta} = a r^n + b \tag{6}$$

$n = 0$ is then called the free-vortex approach. It can be seen in eq. (3) and (4) that the free-vortex approach leads to $c_{2,z} = \mathrm{const.}$ and $p_{2,\mathrm{t}} = \mathrm{const.}$ Therefore this case simplifies the whole design-procedure but has the disadvantage of high flow deflection near the hub. This increases the aerodynamic losses and leads to an increased chord length towards the hub which does in turn drive the axial length of the fan. Apart from these theoretical disadvantages it can be seen both from experiments and CFD that the axial velocity distribution in free-vortex-design fans with high hub-to-tip ratios usually is not radially constant. Figure 3 shows qualitatively the difference between measured and design data for free vortex fans. Because of that the design operating point will probably not be achieved and the process is unreliable. The velocity reductions where examined by different authors, e.g. [2, 6, 7], and can be explained by vortices near hub and tip region. These vortices occur through different effects like the reverse flow at the tip and the stagnation zone behind the hub. Disturbances at the inlet can further increase such effects. [2]

Using a general distribution $r c_{2,\theta} = f(r)$, for example the power-law (eq. 6) with a swirl-exponent of $n = 1$, is called the controlled vortex approach. Such an approach can overcome the disadvantages of the free-vortex distribution by increasing the total pressure rise towards the blade tips. Furthermore a reduction of design total pressure rise at known problematic spots (e.g. tip region) can further increase the accuracy of predictions.

In order to achieve the desired pressure rise Δp_ts, the chosen swirl distribution must be evaluated by integration of eq. (2) from hub to tip radius.

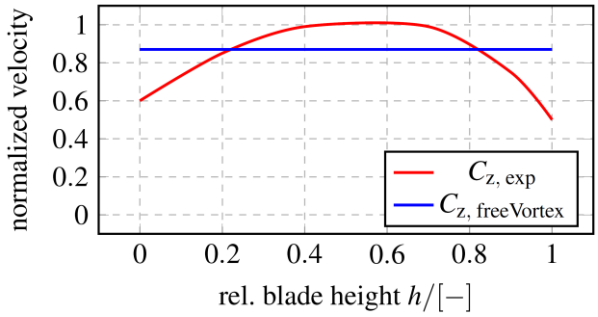

Figure 3: Experimental velocity variation vs. free vortex assumptions

Incidence and Deviation Correction

According to the Euler equation for turbomachinery the work done by a fan blade is a function of the flow-deflection Δc_θ. Therefore it is important to generate blades which satisfy the desired design deflection to the greatest extent possible. The difference between blade-camber-angle (often called "metal-angle") β_m and actual flow angle β is called incidence-angle i or deviation-angle δ respectively and defined as follows:

$$i = \beta_{1,\mathrm{m}} - \beta_1 \quad \text{and} \quad \delta = \beta_{2,\mathrm{m}} - \beta_2 \tag{7}$$

Lieblein carried out many of cascade-experiments to get reliable data for NACA65 airfoils.[3] Because cascade based methods are by definition mostly used for design of medium-to-highly loaded turbomachinery, Lieblein's correlations are restricted to higher solidities and especially higher flow-deflections. In order to get data for low-pressure axial fans, virtual cascades of finite thickness NACA65 profiles were examined using CFD. The virtual domain is shown in pic. 4 and the examined parameter range is listed in table 2.

Table 2: Examined parameter range for finite thickness NACA65 airfoils

Parameter	Range
Incidence angle	-15 to 5°
Camber angle	5 to 25°
Stagger angle	65 to 85°
solidity	0.4 to 1.5

All calculations were done using the open-source toolbox OpenFOAM [8]. The domain consists of a fixed velocity inlet, a pressure outlet, two translational cyclic interfaces and the airfoil itself. The numerical grid is hex-dominant with approximately 250,000 cells and 15 inflation layers around the airfoil. That leads to a dimensionless wall distance of $y^+ \leq 1$. The turbulence-model used was k-ω SST by Menter [9] without additional wall functions.

By changing the inlet-velocity-angle with a fixed magnitude it was possible to analyze different incidence angles under fixed Reynolds number conditions. By evaluating profile loss and deviation angle as a function of geometric parameters and incidence angle, good knowledge about optimal operating conditions is obtained. The dimensionless profile-loss coefficient is therefore defined as follows [10, 11]:

$$\omega = \frac{p_{2,\mathrm{t}} - p_{1,\mathrm{t}}}{p_{1,\mathrm{t}} - p_1} = \frac{\Delta p_\mathrm{loss}}{0.5 \rho w_1^2} \tag{8}$$

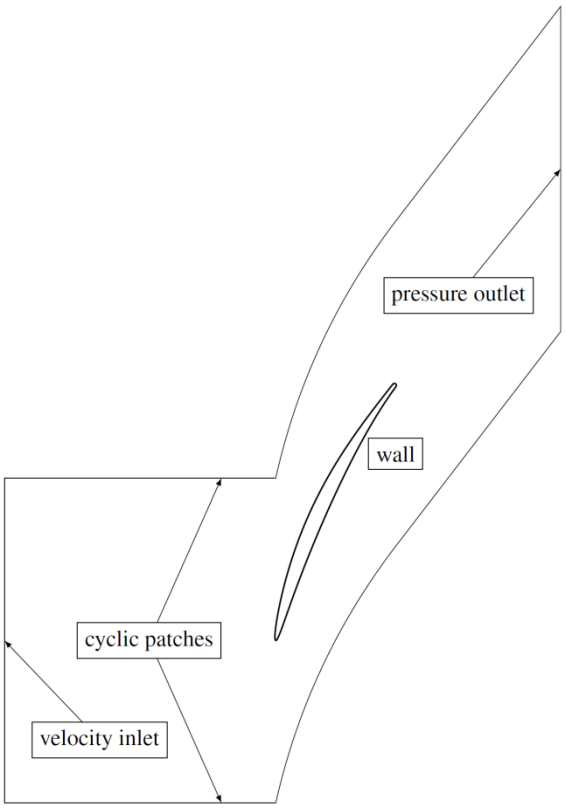

Figure 4: Computational domain for NACA65 cascade analysis

All obtained data was analyzed and combined within one database. Using methods of multidimensional linear interpolation, a continuous response surface model in the form

$$i_{\text{opt}}, \delta, \omega = f(\sigma, \gamma, \Delta\beta) \tag{9}$$

was the result of cascade analysis. i_{opt} is therefore chosen in a way that the loss coefficient $|\omega|$ is minimized. Since the stagger angle γ is a function of the blade angles β_{m} and therefore $\gamma = f(i, \delta, \beta_1, \beta_2)$, the incidence and deviation calculation is done in an iterative way until the stopping criteria $\text{Res}(\gamma) \leq \epsilon$ is reached.

After a detailed analysis of the cascade experiments the results can be summarized as follows: Especially for medium solidities and high stagger angles the aerodynamic losses raise very quickly if optimal incidence is not met. Lower solidities and stagger angles smooth those high gradients and widen the plateau of low losses. Furthermore it has been observed, that lower solidities tend to a relative high negative optimal incidence angle while higher solidities tend to a low negative or even positive incidence angle. Projected on the fan described in table 1, a very sensitive factor within blade design is a good prediction of inflow, especially near the hub, in order to reduce shock losses in medium solidity regions.

Blade Sweep

The need for aeroacoustic-optimized fans has grown rapidly in the last years. Blade-sweep is one of the common tools to decrease acoustic-emissions, especially those caused by disturbed inflow [1, 12]. In the present design-process, the sweep angle $\lambda(r)$ describes the tangential shift of the blade sections in a projection plane normal to the axis of rotation. In terms of the meridional projection no additional shifting is applied. The sweep angle can either be positive (backward sweep) or negative (forward sweep). Carolus and Beiler as well as Corsini and Rispoli showed in their investigations, that forward swept blades can have positive effects on the break-off

point.[12, 13] They explained this effect with the change of meridional velocity distribution due to blade sweep. Backward sweep leads to a distribution shifted towards the blade-tip, while forward sweep does the opposite. Therefore the ratio c_θ/c_z is reduced in hub region.

Since blade sweep has also an influence on the aerodynamics [1, 12, 14], it's important to incorporate blade-sweep and proper aerodynamic load corrections already in the early design stage. Carolus suggested a correlation between reduction in total pressure rise and blade sweep angle λ. [1]

$$dp_\mathrm{t}|_\lambda = dp_\mathrm{t}|_{\lambda=0} \cdot \cos(\lambda)^{0.62} \tag{10}$$

The sweep angle is shown in fig. 5 using an arbitrary point on the stagger line.

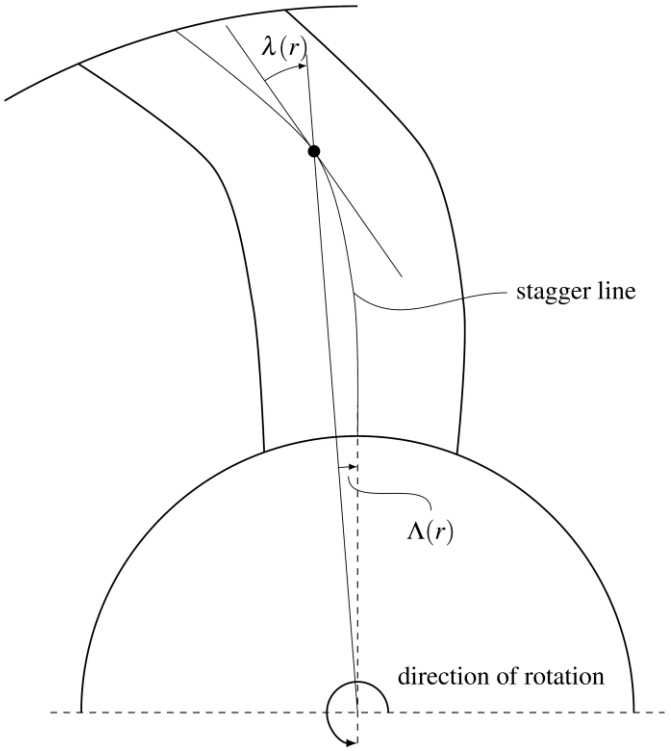

Figure 5: Definition of sweep angle $\lambda(r)$ in a projection plane normal to axis of rotation on a forward swept blade

NUMERICAL SETUP

All simulations are done with formally second order accurate linear upwind differencing schemes (LUDS) using the steady state semi-implicit method for pressure linked equations (SIMPLE). The density of air is assumed to be constant due to low Mach-number and pressure-ratios. The rotor rotation is modelled by adding the coriolis and centrifugal forces as source-terms into the relative Navier-Stokes equations (see eq. (11)). This method is commonly known as the steady state frozen rotor approach and used in many turbomachinery applications. Due to the lack of transient field information, such approaches have the power to predict results at the best efficiency point quite well, as long as no stalling takes place. Other operating points can also deliver reasonable results but those should always be taken with caution, because transient flow-effects could dominate the result and would not be captured by a steady-state approximation. [15]

$$\nabla \cdot (\vec{u}_R \otimes \vec{u}_R) + 2\vec{\Omega} \times \vec{u}_R + \vec{\Omega} \times \vec{\Omega} \times \vec{r} = -\nabla\left({}^{p}/_{\rho}\right) + \nu\nabla \cdot \nabla(\vec{u}_R) \tag{11}$$

The numerical setup of the virtual test rig is shown in pic. 6. The virtual test-rig extends to $8 \times r_\mathrm{tip}$ upwind (suction-chamber) and $18 \times r_\mathrm{tip}$ downstream (pressure-chamber). The cylindrical cross-

section has a radius of $5 \times r_{\text{tip}}$. The numerical grid is generated automatically using the pre-processing software ANSA [16]. The resulting tetrahedral mesh consists of about 50 million cells and is subsequently converted to a polyhedral mesh. The final polyhedral mesh has a total of approximately 13 million cells including at least 4 inflation layers at the rotor.

At the inlet a fixed total pressure condition is applied while the outlet is set to a fixed mean static pressure. All walls except the outer rig boundaries have no-slip conditions (velocity: Dirichlet BC, pressure: Neumann BC). A slip-condition (velocity: mixed Dirichlet/Neumann BC, pressure: Neumann BC) is applied to the outer rig boundaries. The MRF interface must be rotationally symmetric [17] to the axis of rotation and is therefore implemented cylindrically. The interface goes through the middle of the gap between rotor and shroud.

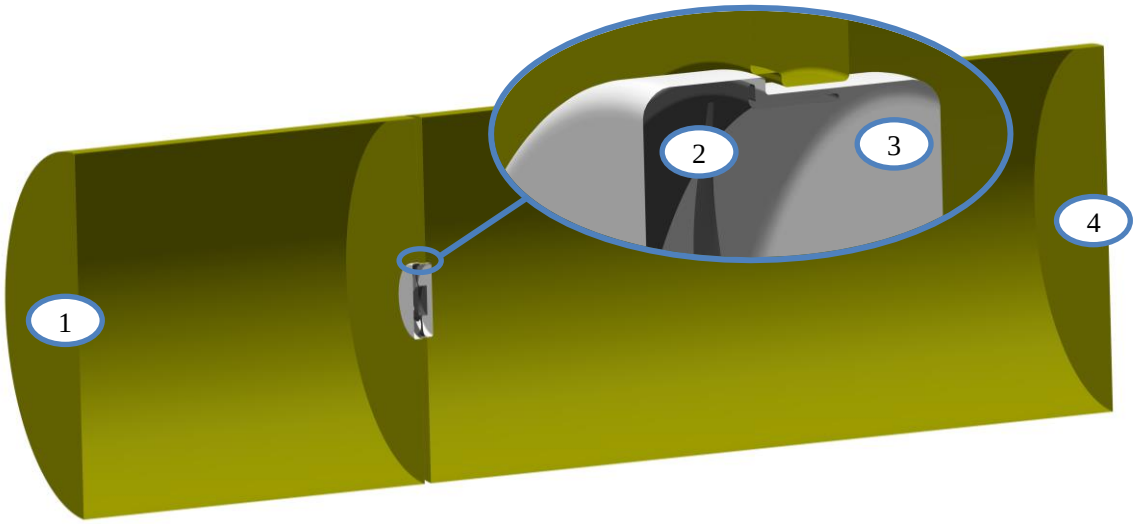

Figure 6: Numerical setup of the virtual test rig (1: inlet, 2: rotor, 3: MRF-interface, 4: outlet)

To ensure reasonable results, each simulation is analyzed in terms of residuals as well as the convergence of integral values. Furthermore the setup was validated with mesh independence analysis and proper reference measurements.

OPTIMIZATION PROCEDURE

In order to maximize the aerodynamic efficiency of the fan blades, a three-dimensional optimization using CFD is applied to the initial design. The objective function is defined as a minimization of shaft-torque

$$\min_{\mathbf{x}\in\Omega} F(\boldsymbol{x}) = \left(M_{z,1}(\boldsymbol{x}), \dots, M_{z,m}(\boldsymbol{x})\right)', \tag{12}$$

where Ω represents the chosen parameter space, $\boldsymbol{x} = (x_1, \dots, x_k)'$ the design variables and $\left(M_{z,1}(\boldsymbol{x}), \dots, M_{z,m}(\boldsymbol{x})\right)'$ the torque in terms of rotational axis in m operating points. Setting $m > 1$ turns the process into a multi-objective optimization in order to deal with off-design points and therefore the integral form of fan curve. The design operating point within a given tolerance is used as a constraint of the optimization.

The whole optimization procedure is based on a response surface model (RSM). Therefore fan blades get parametrized in terms of blade angles at four blade-spans. Additionally the chord length of the whole blade can be varied. The following steps are carried out within the process:

1. generation of design matrix based on Latin Hypercube Design of Experiments (DoE) with nine independent variables

2. carrying out and post-processing of the 3D-CFD simulations
3. generation of a second order RSM based on the simulation results
4. statistical post-processing and evaluation
5. prediction of the global maximum of the RSM using a normal boundary intersection optimization algorithm
6. evaluation of the results

The RSM is based on a second order Taylor polynomial of the form

$$y = \beta_0 + \mathbf{x}'\boldsymbol{\beta} + \mathbf{x}'\mathbf{B}\mathbf{x} + \epsilon, \tag{13}$$

where $\boldsymbol{x}$ contains the independent design variables and $\boldsymbol{\beta}$ the polynomial coefficients

$$\boldsymbol{\beta} = (\beta_1, \dots, \beta_k)' \tag{14}$$

The matrix $\boldsymbol{B}$ is then defined as

$$\boldsymbol{B} = \begin{bmatrix} \beta_{11} & \beta_{12}/2 & \cdots & \beta_{1k}/2 \\ & \beta_{22} & \cdots & \beta_{1k}/2 \\ & & \ddots & \vdots \\ \text{sym.} & & & \beta_{kk} \end{bmatrix} \tag{15}$$

$\boldsymbol{\beta}$ is obtained by the method of least squares in order to include more experiments than actually needed for a second order polynomial.

RESULTS

All results of the design-procedure are shown using typical dimensional characteristics for such fans: flow coefficient φ, total-to-static load coefficient ψ_{ts} as well as the total-to-static hydraulic efficiency η_{ts} using the following definitions.

$$\varphi = \frac{\dot{V}}{\pi \cdot \left(r_{\text{tip}}^2 - r_{\text{hub}}^2\right) \cdot u_{\text{tip}}} \tag{16}$$

$$\psi_{\text{ts}} = \frac{\Delta p_{\text{ts}}}{\rho/2 \cdot u_{\text{tip}}^2} \tag{17}$$

$$\eta_{\text{ts}} = \frac{\Delta p_{\text{ts}} \cdot \dot{V}}{\Omega \cdot M_z} \tag{18}$$

Fans with design characteristics of table 1 were generated

1. … using controlled vortex approach (design 1)
2. … using controlled vortex approach with subsequent 3d-optimization (design 2)

Both fans are forward swept with equal sweep angles. The outer ring and shroud geometry is also the same in both cases. For the optimization process, the blades are subdivided into 4 equally spaced spans. At each radius the camber angles are used as independent variables while the chord length is constant over the whole blade. This results in a total of nine independent variables which are listed for both designs in table 3.

Comparing the parameters of design 1 and 2 it can be noted, that the camber angles do not differ greatly except at the very last radius, where the stagger-angle γ has a large change. It seems that the optimized tip-region can reduce shock-losses and therefore increase the overall efficiency.

Table 3: Blade parameters for two different fan designs

	h	Design 1	Design 2
$\beta_{1,m}$	0.000	29.6°	25.0°
	0.333	9.3°	6.9°
	0.667	8.9°	7.7°
	1.000	5.7°	20.0°
$\beta_{2,m}$	0.000	61.1°	55.1°
	0.333	34.3°	29.4°
	0.667	33.4°	21.1°
	1.000	8.9°	27.7°
c	0 to 1	0.07 m	0.064 m

The characteristics of both fans are shown in fig. 7. Unless otherwise specified, all curves are based on the virtual fan test rig. Figure 7 shows the total-to-static load coefficient and the total-to-static hydraulic efficiency in terms of flow coefficient. Both designs predict the design point very well. Looking at the off-design region, design 1 generates a higher pressure rise in the partial load region while design 2 has a higher pressure rise at higher flow rates. The maximum hydraulic total-to-static efficiency of the optimized fan is predicted to be nine percentage points higher than of the initial design. Furthermore the best efficiency point of design 2 is shifted slightly towards higher flow rates, but both designs have their best efficiency close to the design point.

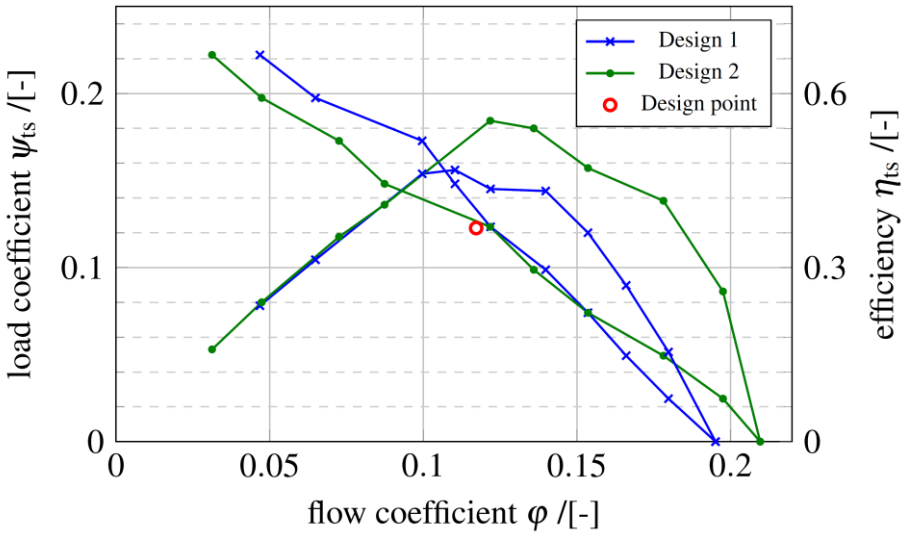

Figure 7: Dimensionless characteristics for two different rotor designs

The design 2 fan has been built and tested experimentally. The test facility of the TU Braunschweig was used, which is an inlet-side test chamber setup according to DIN/ISO5801 [18]. In order to measure the whole fan curve, a throttle is used to increase the resistance and therefore the necessary pressure rise. Figure 8 shows the measured fan curve in comparison with the simulated one. As it can be seen, the differences between simulated and measured data are small. Even points in the partial loading region are captured well in CFD. Therefore it can be remarked, that the overall

characteristics of both are very close. Even if the efficiency characteristics are also captured very well, the simulated maximum is slightly shifted towards lower flow-rates.

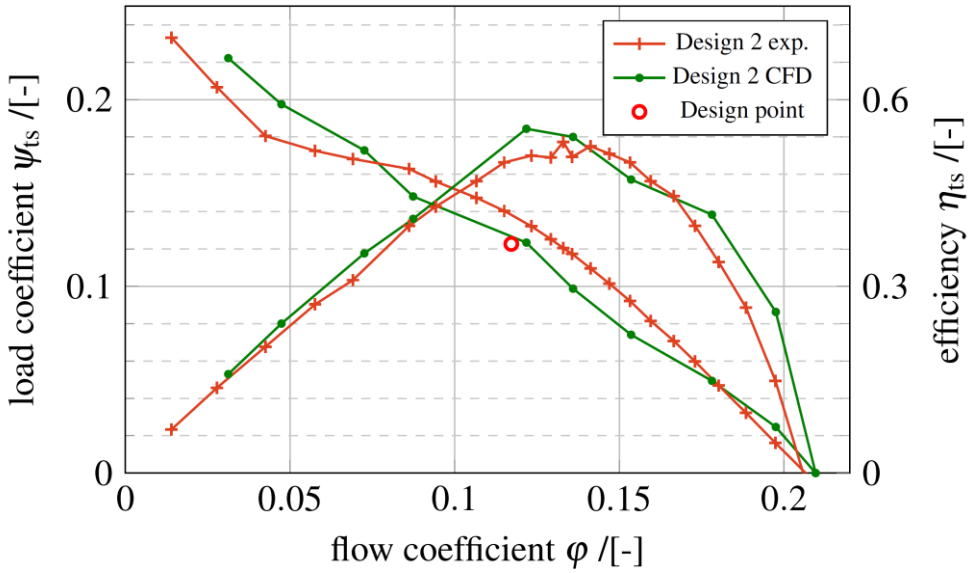

Figure 8: Comparison of experimental data vs CFD results for design 2

SUMMARY AND CONCLUSION

Modern HVAC-type axial fans need the best possible aerodynamic efficiency and low aeroacoustic emissions. Furthermore due to short product-cycles, the design procedure has to be fast and reliable. Therefore different design-methods for low-pressure rotor only axial fans were discussed. Those fans are used for a wide range of HVAC applications and often have low-to-medium solidities. In that case the literature commonly refers to using the isolated airfoil approach with additional corrections to take interference effects into account. The presented design-procedure uses a cascade based design instead. Some important aspects to get reliable results were presented. In particular incidence and deviation correction, influence of blade-sweep and effects of design vortex-distribution were described. Additionally a response surface based optimization procedure was presented for further three-dimensional optimization.

Finally two different fans were generated using the controlled vortex approach and the controlled vortex approach with subsequent optimization. The fan-curves were presented and discussed. The controlled vortex design fan shows good characteristics and meets the required operating point. Design 2 uses the first one as starting point for subsequent optimization. This design shows an increased efficiency because three-dimensional effects like vortices at hub and tip are captured within the optimization using 3D-CFD. In order to validate that design, a prototype has been built and tested in test facilities of the TU Braunschweig. The measured data shows good agreement with the predicted characteristics.

Altogether it can be remarked, that a fully virtual cascade-based procedure has been presented with the aim of designing high efficiency low-to-medium solidity fans with blade-sweep. This process is very flexible in terms of 2d-profiles since the database can be quickly adjusted by using virtual two-dimensional cascade experiments. Additionally such a database has the advantage that losses can be calculated directly and therefore no additional assumptions regarding profile losses have to be made. Regarding further three-dimensional optimization it has been shown, that a response surface model based process has the power to generate high efficiency fans within a short development time.

BIBLIOGRAPHY

[1] Thomas Carolus – *Ventilatoren: Aerodynamischer Entwurf, Schallvorhersage, Konstruktion.* Vieweg+Teubner Verlag, **2013**

[2] Bruno Eck – *Ventilatoren: Entwurf und Betrieb der Radial-, Axial- und Querstromventilatoren*, Sechste Auflage. Klassiker der Technik. Springer, Berlin, Heidelberg, **2003**

[3] Members of the Staff of Lewis Research Center – *Aerodynamic design of axial-flow compressors.* In: NASA SP-36, **1965**

[4] R. A. Wallis – *A rationalised approach to blade element design, axial flow fans.* In: Proc. of the third Australasien Conference on Hydraulic and Fluid Mechanics, Sydney, **1968**

[5] J. H. Horlock, H. Marcinowski – *Axialkompressoren.* Wissenschaftliche Bücherei Reihe Strömungstechnik. Braun, Karlsruhe, **1967**

[6] L. Bommes – *Ventilatoren*, 2. Aufl. Vulkan-Verl., Essen, **2003**

[7] T. B. Lindemann – *Optimale Niederdruck-Axialventilatoren für den Einsatz bei kleinen Reynoldszahlen: Abschlussbericht*, Forschungsvereinigung für Luft- und Trocknungstechnik e.V., vol 224. FLT, Frankfurt, **2010**

[8] H. G. Weller, G. Tabor, H. Jasak et al. *A tensorial approach to computational continuum mechanics using object-oriented techniques.* In: Computers in Physics., **1998**

[9] F. R. Menter – *Two-equation eddy-viscosity turbulence models for engineering applications.* In: AIAA Journal 32.8, **1994**

[10] R.I. Lewis – *Turbomachinery performance analysis.* Arnold, London, **1996**

[11] M. T. Schobeiri – *Turbomachinery flow physics and dynamic performance*, 2. and enhanced ed. Springer, Berlin, **2012**

[12] M. G. Beiler, T. H. Carolus – *Computation and Measurement of the Flow in Axial Flow Fans With Skewed Blades.* Journal of Turbomachinery, **1999**

[13] A. Corsini, F. Rispoli – *The Role of Forward Sweep in Subsonic Axial Fan Rotor Aerodynamics at Design and Off-Design Operating Conditions.* In: ASME Turbo Expo 2003, collocated with the 2003 International Joint Power Generation Conference, **2003**

[14] T.B. Lindemann, J. Friedrichs, U. Stark – *Development of a New Design Method for High Efficiency Swept Low Pressure Axial Fans With Small Hub/Tip Ratio*. In: ASME Turbo Expo 2014: Turbine Technical Conference and Exposition, **2014**

[15] A. Corsini, G. Delibra, A. G. Sheard – *A Critical Review of Computational Methods and Their Application in Industrial Fan Design.* ISRN Mechanical Engineering, **2013**

[16] BETA CAE Systems – ANSA - *The advanced CAE pre-processing software for complete model build up*. http://www.beta-cae.com/ansa.htm, **2017**

[17] ANSYS (2013a) – *FLUENT Theory Guide.* Version 15.0, **2013**

[18] International Organization for Standardization – ISO 5801:2017 *Fans -- Performance testing using standardized airways.* ISO, **2017**